

Sparse Deconvolution Methods for Online Energy Estimation in Calorimeters Operating in High Luminosity Conditions

Tiago Teixeira^a Luciano Andrade^a José Manoel de Seixas^b

^a*Electrical Engineering, Federal University of Juiz de Fora,
Minas Gerais, Brazil*

^b*Signal Processing Lab, COPPE/POLI - Federal University of Rio de Janeiro,
Rio de Janeiro, Brazil*

E-mail: tiago.teixeira@engenharia.ufjf.br

ABSTRACT: Energy reconstruction in calorimeters operating in high luminosity particle colliders has become a remarkable challenge. In this scenario, pulses from a calorimeter front-end output overlap to each other (pile-up effect), compromising the energy estimation procedure when no preprocessing for signal disentanglement is accomplished. Recently, methods based on signal deconvolution have been proposed for both online and offline reconstructions. For online processing, constraints concerning fast processing, memory requirements, and cost implementation limit the overall performance. Offline reconstruction allows the use of Sparse Representation (SR) theory to implement sophisticated Iterative Deconvolution (ID) methods. This paper presents ID methods based on SR algorithms whose computational cost is effective for online implementation. Using simulation data, current techniques were compared to the proposed SR ones for performance validation in the online environments. Analysis has shown that, despite the higher computational cost, when compared to standard methods, the increase in performance may justify the use of the proposed techniques, in particular for the Separable Surrogate Functional (SSF). which is shown to be feasible for implementation in modern FPGAs.

KEYWORDS: Deconvolution, Online Energy Estimation, Sparse Representation, Calorimetry

Contents

1	Introduction	1
1.1	The Pile-up Effect	2
1.2	Windowed Vesurs Sample-by-Sample Implementation	3
1.3	The SR Algorithms	4
2	FIR Filter Based Energy Estimation	4
3	Proposed SR Based Deconvolution Methods	5
3.1	Matching Pursuit - MP	6
3.1.1	Orthogonal Matching Pursuit	7
3.1.2	Least-Squares Orthogonal Matching Pursuit	7
3.2	Iterative-Shrinkage	7
3.2.1	SSF Initialization	8
4	Results	9
4.1	FIR Filter Design	10
4.2	MP Parameters	10
4.3	SSF Parameters	11
4.4	Estimation Performance	12
4.5	Detection Efficiency	14
4.6	Analysis Summary	15
5	Hardware Implementation	15
5.1	System Evaluation	17
5.2	FPGA Implementation	18
6	Conclusion	19

1 Introduction

High Energy Physics (HEP) experiments usually require sophisticated instrumentation systems, especially when particle colliders are involved [1]. In order to analyze increasingly rare physical phenomena, there is a tendency of increasing their collision rates and the number of particles per collision, thus increasing the luminosity achieved by the experiment [2]. This is the case of the most potent collider ever built, the LHC (Large hadron Collider) [3] at CERN (*Organisation Européenne pour la Recherche Nucléaire*) [4]. The LHC collides bunches of protons at each 25 nanoseconds and has been establishing records in terms of both collider energy and luminosity [5]. Moreover, upgrades that are on the way for the next LHC operation periods (Run 3 and beyond) will increase even more the luminosity [6], towards a projected peak around $5 \text{ to } 7.5 \times 10^{34} \text{ cm}^{-2} \text{ s}^{-1}$ [7].

For new physics identification at LHC, calorimeters [8] play an important role, as they measure the energy of the incoming particles and are essential for triggering purposes [9]. The two general-purpose LHC experiments (ATLAS [10] and CMS [11]) comprise hundred of thousands calorimeter readout channels each and employ state-of-art detector technology. However, the LHC’s enormous luminosity imposes severe restrictions on calorimetry performance, as despite being fast, the signal generated in the detector’s front-end electronics requires a certain number of bunch crossings (BCs) to be fully developed. Therefore, signal pile-up effects may arise when the luminosity is increased.

The trigger system is often implemented through an online cascade signal processing chain consisting of two or more levels, where the rate reduction is proportional to the level of the algorithm complexity for final event selection. Due to the high event rate, the lower filtering levels are usually implemented in hardware and rely very much on online energy estimation, which is addressed in this paper for applications where signal pile-up becomes an issue.

1.1 The Pile-up Effect

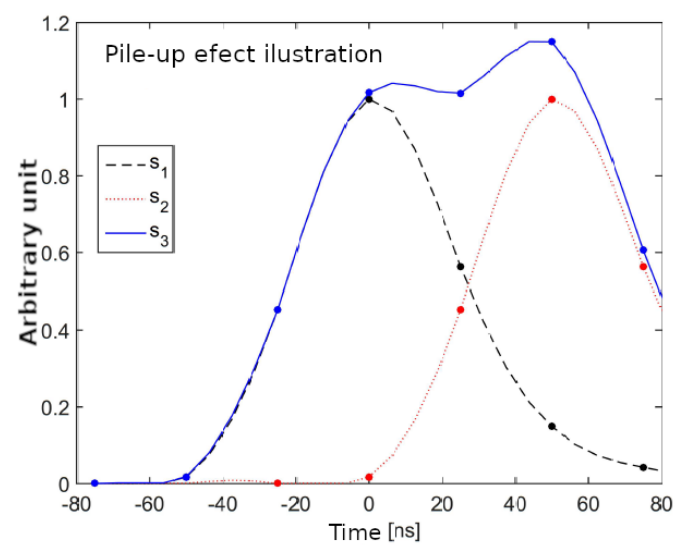


Figure 1: Example of the pile-up effect. See text.

An example of out-of-time signal pile-up in collider experiments can be seen in Figure 1, where signals were digitized by a 40 MHz clock (25ns period, as in the LHC). The unipolar signal generated in a hypothetical calorimeter cell by a given collision is referred to as s_1 , and 50ns later a new signal (s_2) from two bunch crossing collisions after reaches that particular cell. Supposing a 150ns readout acquisition window length, the s_3 signal is formed, which is actually the stacking of both s_1 and s_2 signals. This pile-up effect leads to a sub-optimal operation of the classical energy estimation algorithms, which are based on Optimal Filtering (OF) theory [12–15].

Recently, a novel deconvolution-based approach has been proposed for mitigating the pile-up effect [16]. This method has shown to outperform standard OF methods when signal pile-up can not be neglected. Since the calorimeter signal shape overlapping is a linear procedure and the signal amplitude is proportional to the target energy value [8], the sensor output can be modeled as the convolution between the target sequence (energy deposition per BC) and the calorimeter

normalized (unitary amplitude) reference pulse shape. Therefore, to recover the target sequence, a deconvolution algorithm may be applied [17]. Different deconvolution algorithms were proposed for energy estimation in high-luminosity calorimeter operation. The work in [16] proposes an offline procedure in two steps, where a signal detection per BC is performed first, followed by a multi-amplitude estimation procedure.

Still focusing on offline reconstruction, the work in [18] implements an approach based on Sparse Representation (SR) [19] of data, presenting remarkable results, over-performing standard deconvolution methods. SR was originally developed and applied in signal compression and image denoising routines [20, 21]. The work in [18] inaugurated the SR energy reconstruction applications. However, its cost implementation is presently forbidden for online data-stream.

Concerning online processing, a deconvolution method based on Finite Impulse Response (FIR) [22] filters was proposed in [23] and it has shown to be very attractive due to its lower cost implementation in hardware. However, recently SR theory has developed families of algorithms targeting cost implementation reduction [24–26]. Although FIR filter structures are known to be the most economic approach in terms of hardware resources, the cost-effectiveness of such modern SR techniques has paved the way for online energy reconstruction implementation. Those approaches have already been used in several online applications like machine learning [27] and big data [28].

1.2 Windowed Versus Sample-by-Sample Implementation

Concerning hardware implementation, SR and FIR filters comprise very different approaches. The latest presents its output signal in a sample-by-sample fashion, which is very suitable and straightforward for free-running environments. On the other hand, SR algorithms operate simultaneously on all the samples previously buffered within a window. Actually, this non-causal characteristic is one of the reasons of the increasing in performance, when compared to the FIR filter structures. Therefore, operating a windowed energy reconstruction algorithm in a free-running environment is one of the challenges resolved in the present work. The online implementation of windowed methods demands extra digital circuitry for proper data-flow. In this paper, the proposed SR methods are first demonstrated. Then, a hardware solution for online implementation is outlined.

Actually, the adaptation of such a non-causal method to online operation is possible thanks to some characteristics of modern colliders, like the LHC. In this experiment, operation in a train-of-bunches may be required [29, 30]. Due to particle injection stability issues, the accelerator needs small periods of empty-bunches intercalated with periods of bunch-trains [31]. At Run 2, for instance, typical physics runs have been operated in a configuration of 48 filled bunches followed by 7 (or more) empty bunches [32]. It turns out that this issue encourages the use of windowed estimation methods as the ones proposed here, since such an operational approach eliminates two important design difficulties:

1. **Window size determination** - in adapting windowed methods to free-running environments, the window size is to be determined. In a train-of-bunches configuration, it is natural to choose the window size in order to fit an entire train within the processing window.
2. **Border effect** - A problem found in the windowing signal processing is that signals on the window border are split into neighbor windows. As a consequence, the estimation of

BCs closer to the window edge tends to reduce the processing efficiency. However, due to the train-of-bunches configuration, providing that the calorimeter reference signal width is smaller than the empty-bunches period, the border effect does not occur.

In this paper, bunch-trains of 48 bunches followed by 7 empty bunches were used. Thus, window lengths of 54 bunches (48 central plus the guard comprising three bunches in each side of the window) were employed to avoid the border effect.

1.3 The SR Algorithms

The most efficient implementation of SR methods is based on Linear Programming (LP) [33], which is a very low cost-effective procedure [34] and, thus, indicated for offline processing only. Among the cost-effective algorithms, Matching Pursuit (MP) methods [35] have an intrinsic relationship with energy estimation tasks. In MP, a signal detection iterative procedure is executed first, using a bank of linear Matching-Filter (MF) [36] based filters. After some iterations, all the superimposed signals within an acquisition window are detected. Their amplitudes are, then, estimated simultaneously using the Least Square (LS) algorithm [37].

Another SR family of methods that is being employed due to its excellent cost-benefit properties is the Iterative-Shrinkage (IS) algorithms [38]. These methods combine standard linear Coordinate-Descent (CD) algorithms [39] with a linear-by-part Shrinkage function in order to promote sparsity, becoming one of the most cost-effective algorithms for SR.

Therefore, the main goal of this paper is to use modern SR theory in a design that is capable of operating online. The adaptation of some of those techniques is proposed envisaging energy estimation in calorimeter cells, opening a new research area in online energy reconstruction. Since SR has shown to be the most accurate energy reconstruction procedure under pile-up, the methods proposed here can be used as an alternative for FIR filter implementation in applications where the hardware resources minimization is not a main constraint. A comparison, among the aforementioned methods, in terms of cost implementation and energy reconstruction performance, is provided in this paper, indicating the best situation for the usage of each approach.

In order to complete the discussion, a possible implementation for one of the proposed SR methods (SSF) is outlined at the end of this paper. The circuitry was developed in Hardware Description Language (HDL) [40] envisaging a straightforward implementation in modern FPGAs.

2 FIR Filter Based Energy Estimation

Figure 2 shows the basic structure for online energy estimation based on a FIR deconvolutional filter [23]. The signal $r[n]$ represents the measured information from a single calorimeter sensor front-end output, after applying the free-running (an uninterrupted) Analog-to-Digital Converter (ADC). A cascade of registers, synchronous with the ADC clock, implements a shift-register structure [40], which is responsible for storing the latest M digitized samples. The filter order ($M-1$) depends on both the calorimeter reference pulse-shape width and the signal pile-up intensity. For deconvolution, the filter order is often higher than the reference pulse width (two times on average), since the filter needs tail information of neighbor superimposed signals to perform the desired source separation. The equation employed in this deconvolution procedure is:

$$x'[n] = \sum_{l=0}^{M-1} (w[n-l]r[n]) \quad (2.1)$$

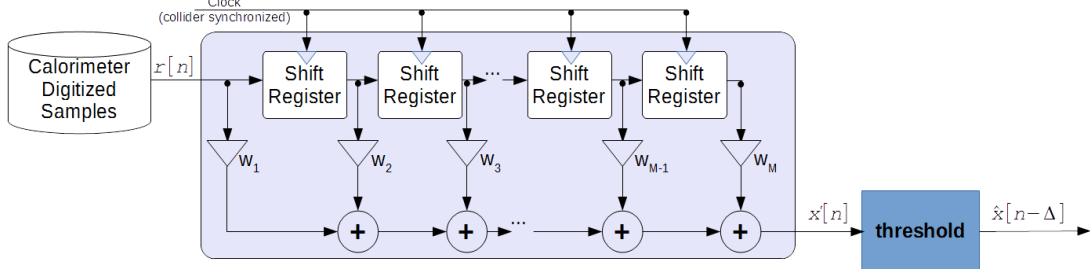


Figure 2: The FIR filter structure implementing signal deconvolution in online energy estimation, based on [23].

The weighting vector \mathbf{w} is computed offline, based on deconvolution principles. Details on the filter design can be found in the original paper [23]. The samples are, then, linearly combined at the filter output, which delivers a new information at each clock. A threshold is applied on the filter output to avoid small artifacts from the deconvolution process in adjacent BCs, mainly small negative energy estimations.

The system output corresponds to the reconstructed target information sequence $\hat{x}[n]$, which is a straightforward estimation of the energy deposit per BC ($x[n]$). The system starts delivering the output sequence Δ clock cycles after the first sample goes through the processing chain and the corresponding estimate is outputted. This delay is necessary because the system needs information from previous samples in order to promote the deconvolution procedure. Typical values of Δ are around half of the filter order.

Despite of its very suitable hardware implementation, the purely linear operation of FIR filters does not allow to access the Higher Order Statistics (HOS) [41] present in the embedded pile-up noise, which may be exploited for further performance improvement. The proposed SR based deconvolution methods access the HOS information indirectly through the usage of non-linear functions in the deconvolution process.

3 Proposed SR Based Deconvolution Methods

Different from the previously described technique, SR-based deconvolution methods are designed using a windowed acquisition point of view. The method is guided by the matrix formulation for the convolution operation of finite size sequences, as proposed in [18], and quoted in Equation 3.1. Given a normalized calorimeter reference pulse-shape, represented by the vector \mathbf{h} of size V and a target sequence, represented by the vector \mathbf{x} (energy per BC) of size G , the convolution between these two signals (the measured signal) is the calorimeter sensor readout \mathbf{r} sequence of size $U = V + G - 1$ [22].

$$\mathbf{r} = \mathbf{H}\mathbf{x} \quad (3.1)$$

where \mathbf{H} is the convolution matrix of size $U \times G$ (columns of \mathbf{H} contain shifted versions of the vector \mathbf{h} , with zero padding). The windowed deconvolution procedure consists of recovering the sequence \mathbf{x} when \mathbf{r} is measured and \mathbf{H} is known. When the size of the vector \mathbf{r} is greater than the one of \mathbf{x} , there are infinite solutions for this system of equations. In [18], it was shown that, for deconvolution purposes, the sparsest representation of \mathbf{x} is the correct solution when the target sequence is characterized by impulsive signals.

According to the SR theory [19], the sparsest solution for Equation 3.1 can be found solving the optimization Problem P_ℓ for $0 \leq \ell \leq 1$

$$(P_\ell) : \min_{\mathbf{x}} \|\mathbf{x}\|_\ell^\ell \text{ subjected to } \mathbf{r} = \mathbf{H}\mathbf{x} \quad (3.2)$$

where

$$\|\mathbf{x}\|_\ell^\ell = \sum_b |x_b|^\ell \quad (3.3)$$

is the ℓ -norm of the vector \mathbf{x} .

For $\ell = 1$, this results in a typical LP problem [33]. The use of LP for SR aiming at energy estimation has been outlined in [18], where this method was shown to outperform other windowed deconvolution methods. However, the focus of that paper was for offline energy reconstruction, since LP presents a very high computational cost, becoming usually prohibitive for online execution. In the sequence, two families of SR algorithms are presented in order to solve the P_ℓ problem with different perspectives, both focusing on computational cost-effectiveness procedures.

3.1 Matching Pursuit - MP

For $\ell = 0$, Equation 3.3 results in the number of non-zero elements in \mathbf{x} and the SR solution given by P_0 becomes evident. However, P_0 is not a mathematically tractable problem [19]. This is a combinatorial problem unfeasible to be implemented computationally in practice.

To avoid the test of all combinatorial possibilities, MP seeks for similarities between columns of the matrix \mathbf{H} and the vector \mathbf{r} , selecting the smallest number of columns that, when linearly combined, produce the vector \mathbf{r} added to a small residue vector \mathbf{d} .

Given the support matrix \mathbf{H}_s , which comprises the selected columns of \mathbf{H} , the residue vector \mathbf{d} is

$$\mathbf{d} = \mathbf{H}_s \mathbf{x}_s - \mathbf{r} \quad (3.4)$$

where the vector \mathbf{x}_s has the amplitudes for each signal in \mathbf{H}_s (the columns of \mathbf{H}_s). The components in \mathbf{x}_s are chosen in order to minimize the square module of the residue:

$$\epsilon^2 = \mathbf{d}^T \mathbf{d} = |\mathbf{H}_s \mathbf{x}_s - \mathbf{r}|^2 \quad (3.5)$$

where T indicates a vector transposition.

The vector \mathbf{x}_s that minimizes the Equation 3.5 is obtained by the least-square equation (LS)

$$\mathbf{x}_s = (\mathbf{H}_s^T \mathbf{H}_s)^{-1} \mathbf{H}_s^T \mathbf{r} \quad (3.6)$$

The MP algorithms select columns of the matrix \mathbf{H} with the highest potential of minimizing ϵ^2 [42]. Depending on the way this task is performed, a specific variation of the basic MP algorithm is applied. In this work, the Orthogonal MP (OMP) [43] and the Least Square OMP (LS-OMP) [44] will be outlined.

3.1.1 Orthogonal Matching Pursuit

This method selects the column \mathbf{h}_j of the matrix \mathbf{H} that best matches the current residue \mathbf{d} , minimizing the cost function

$$Q(x_j) = |x_j \mathbf{h}_j - \mathbf{d}|^2 \quad (3.7)$$

The value x_j that minimizes this function is the MP equation

$$x_j = \frac{\mathbf{h}_j^T \mathbf{d}}{\mathbf{h}_j^T \mathbf{h}_j} \quad (3.8)$$

This value is computed for all \mathbf{h}_j columns not yet inserted in the support matrix \mathbf{H}_s . The column with the smallest $Q(x_j)$ value is selected, the new residue vector is computed and a new iteration is performed until ϵ becomes lower than a given threshold ϵ_0 . It can be shown [44] that all the columns of \mathbf{H}_s are orthogonal to the remaining residue \mathbf{d} .

3.1.2 Least-Squares Orthogonal Matching Pursuit

The LS-OMP method updates temporarily \mathbf{H}_s with the current column \mathbf{h}_j in test and computes ϵ directly (Equation 3.5). The temporary matrix \mathbf{H}_s that gives the smallest ϵ value is kept. The process stops when current residue is lower than ϵ_0 as well. Different from OMP, which computes a simple inner product (MP equation) to each column not yet inserted in \mathbf{H}_s , LS-OMP computes the LS (Equation 3.6) instead. Therefore, the computational cost of LS-OMP is higher than OMP.

3.2 Iterative-Shrinkage

IS algorithms are based on the Problem P_1 . However, a relaxation is employed in order to allow a small residue square error ϵ_0 on the constraint.

$$(P_{1,\epsilon_0}) : \min_{\mathbf{x}} \|\mathbf{x}\|_1 \text{ subjected to } |\mathbf{H}\mathbf{x} - \mathbf{r}|^2 < \epsilon_0 \quad (3.9)$$

The problem P_{1,ϵ_0} is a typical LP problem, as directly performed in [18] for offline signal reconstruction. However, focusing on cost-effectiveness, firstly, this problem is transformed in an optimization routine without constraint by the use of a Lagrange multiplier λ [19]

$$(P_{1,\lambda}) : \min_{\mathbf{x}} \|\mathbf{x}\|_1 + \lambda |\mathbf{H}\mathbf{x} - \mathbf{r}|^2 \quad (3.10)$$

where ϵ_0 is absorbed by λ . The IS algorithms propose solving Problem $P_{1,\lambda}$ by means of iterative CD methods: given an initial guess vector \mathbf{x}^0 , the optimal \mathbf{x}_{opt} value can be recursively inferred in a small number of steps. However, the use of standard CD methods, like Newton-Raphson [45], becomes prohibitive for $P_{1,\lambda}$ because of the discontinuity of the ℓ -norm for $\ell = 1$ [19].

In [46], the insertion of terms in $P_{1,\lambda}$ is proposed, so that the minimum coordinate position \mathbf{x}_{opt} is not changed, but the multivariate problem is split into separated one-dimensional problems, which can be solved by parts. The resulting equation is named as Surrogate Function, and the respective IS method is the Separable Surrogate Functionals (SSF). After some algebraic manipulation, the iterative procedure can be compacted as follows

$$\mathbf{x}^{i+1} = \Gamma_{\lambda} \left(\mathbf{x}^i + \mu [\mathbf{H}^T (\mathbf{r} - \mathbf{H}\mathbf{x}^i)] \right) \quad (3.11)$$

where μ is the step size in the direction to the minimum. The function $\Gamma_{\lambda}(\theta)$ is the one-dimensional shrinkage function that should be applied to each component of the vector \mathbf{x} . In this paper, a modification on the shrinkage function is proposed in order to promote positive energy estimation, as shown in Figure 3. With this modification, the resulting function can be simply implemented through a subtraction followed by a threshold (λ) operation. The argument in Equation 3.11 is identified as a linear Gradient-Descent (GD) iteration [47] and comprises only addition and multiplication operations. The parameters μ and λ are both obtained from simulation.

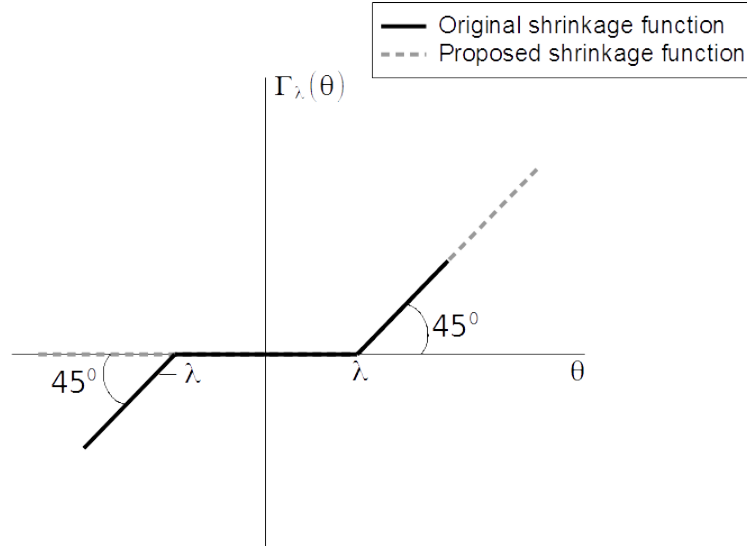


Figure 3: The original shrinkage function and the proposed modified version to promote positive energy estimation.

3.2.1 SSF Initialization

One important prerequisite for online implementation of the SSF algorithm is to avoid a higher number of iterations. This can be accomplished by choosing a proper initial vector \mathbf{x}^0 . In this work, a pre-processing routine is proposed, in order to initialize the solution close to the optimal one. The proposal is to implement the LS (Equation 3.6) for a full-support matrix \mathbf{H} :

$$\mathbf{x}^0 = (\mathbf{H}^T \mathbf{H})^{-1} \mathbf{H}^T \mathbf{r} = \mathbf{H}^+ \mathbf{r} \quad (3.12)$$

where $\mathbf{H}^+ = (\mathbf{H}^T \mathbf{H})^{-1} \mathbf{H}^T$ is the pseudo-inverse of matrix \mathbf{H}^T [48]. This is a constant matrix, which may be obtained offline.

4 Results

In order to validate the proposed algorithms, a toy Monte Carlo simulation was used for generating a set of consecutive samples, which represent the target energy values, per BC, for a single readout channel. Energy distributions and sensor's front-end were simulated following the characteristics found in modern calorimeters [49–51].

The pile-up effect was assessed through the calorimeter cell occupancy: null occupancy corresponds to the absence of hits in a given run and on the other extreme, 100% of occupancy means that an amount of energy is deposited at every particle collision.

Without loss in the generality, the cell calorimeter shaped pulse was considered as unipolar [52–54], Gaussian-like, with an acquisition window of 150 ns. The collision rate was of 40 MHz (as in the LHC), resulting in a seven-sample pulse representation (analogue-to-digital clock was synchronous with the collider bunch spaces) where the pulse peak corresponded to the central sample (4th sample). It is worth mentioning that the proposed method might be applied to any pulse shape, provided it represents the impulse response ($h[n]$) to be deconvolved.

The simulation framework employed here was also used in recent related works [18, 23], where more details can be found. The signal characteristics were:

- The occupancy range: from 1% to 90%, in steps of 10%.
- Energy deposition: from an exponential distribution of 360 MeV.
- Phase shift: an uniformly random pulse-phase in the range ± 1 ns is employed to each generated signal.
- Electronic noise: zero-mean white Gaussian noise with $\sigma = 15$ MeV.

For performance comparisons, signal data from 1,820 windows were considered, forming a data stream with 100,100 samples. The simulation data were split into ten subsets of ten thousand and ten events each, in order to evaluate the statistical fluctuations. The error bars were computed through a cross-validation procedure [55]. In this procedure, one subset was kept for testing and did not participate in the filter design, which used the remaining nine subsets. The testing subset was shifted for each fold, so that each subset could play once the role of the testing subset along the cross-validation procedure. The average performance and the Root Mean Square (RMS) value from the ten models developed along such a procedure were computed as the estimate of the expected performance and the corresponding error bar, respectively.

For optimal parameter determinations and for performance evaluations, the RMS of the error between the target ($x[n]$) and the estimated ($\hat{x}[n]$) sequences was employed (Equation 4.1)

$$RMS\ Error = \sqrt{\frac{\sum_{n=1}^N (\hat{x}[n] - x[n])^2}{N}} \quad (4.1)$$

where N was the total number of samples in the test set (10,010).

4.1 FIR Filter Design

The baseline implementation was proposed in [23] (see Figure 2). For filter design, two parameters must be tuned: the filter order and the threshold value for reducing the estimation error.

The energy estimation performance as a function of the filter order is shown in Figure 4. In this figure, the output threshold was set to null aiming at avoiding negative energy estimations. Based on this figure, a filter order of 22 was kept fixed for further analysis (hence, the filter delay was $\Delta = 11$ samples), regardless the occupancy value, since the RMS error did not decrease for higher filter order values. For optimal threshold value determination, the estimation error as a function of the threshold value is plotted in Figure 5 for each occupancy value. One can conclude that a threshold around 30 MeV might be used regardless the occupancy level. As expected, the estimation error increased with the pile-up level.

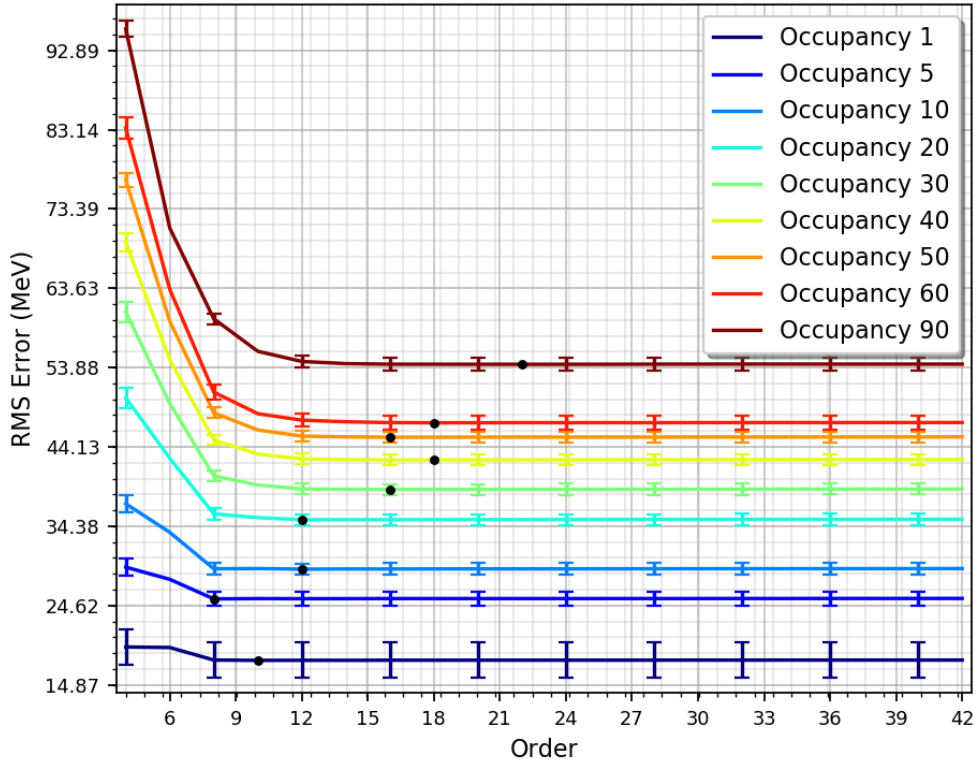


Figure 4: The estimation error as a function of the FIR filter order (threshold set as zero). The black dots point out the FIR Filter order values for which the minimum RMS errors were achieved.

4.2 MP Parameters

The unique parameter to be determined for the MP methods is the squared value for the residue limit (ϵ_0^2). Figure 6 shows such error limits as a function of this parameter for both the OMP and the LS-OMP methods. Since this parameter is measured in MeV^2 , its squared root value was employed for the sake of physical interpretation in terms of energy values in MeV. As expected, the optimal residue value decreased as the occupancy level was increased, requiring more signals in the support matrix \mathbf{H}_s . Although both methods achieved similar performance, it is worth mentioning

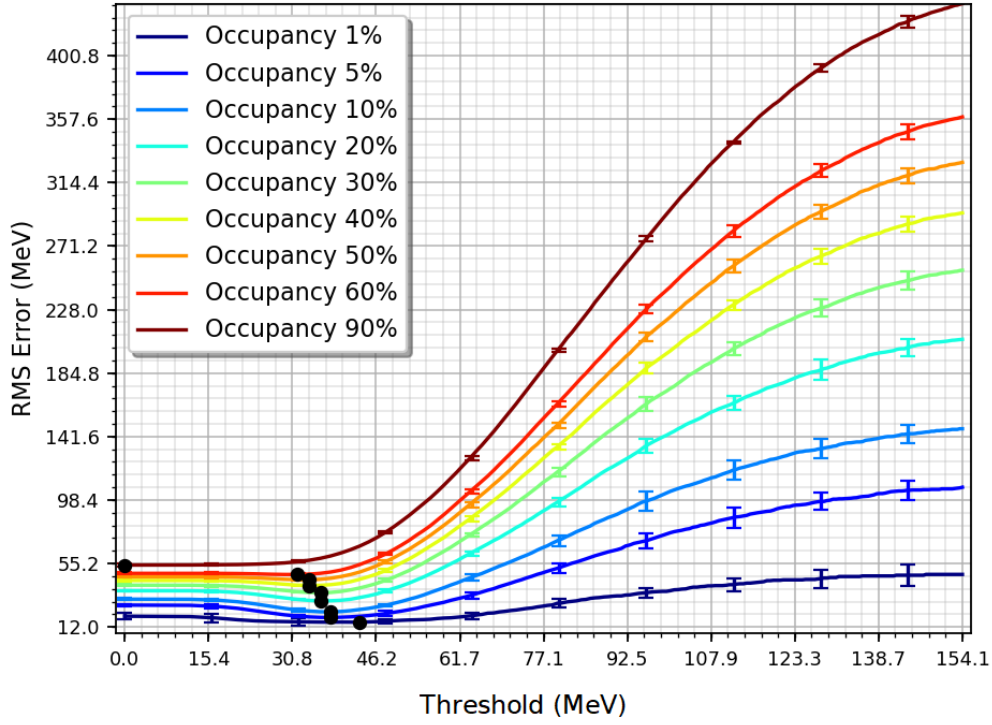


Figure 5: The estimation error as a function of the threshold value determined in the output of the FIR filter. The black dots point out the threshold values for which the minimum RMS errors were achieved.

that the amount of operations for LS-OMP implementation is much higher, as it executes a complete estimation with LS for each iteration whereas the OMP method applies the linear regression only at the final stage.

4.3 SSF Parameters

For SSF, two parameters require tuning: the step-size μ for the CD iterations and the λ value for the shrinkage function. For faster convergence, the μ value may be determined dynamically, depending on the current residue \mathbf{d} . Since the argument in Equation 3.11 is a linear GD iteration step, the optimal step-size μ for the i -th iteration is [56]

$$\mu = \frac{\mathbf{d}^{iT} \mathbf{d}^i}{\mathbf{d}^{iT} (\mathbf{H}^T \mathbf{H}) \mathbf{d}^i} \quad (4.2)$$

where $\mathbf{d}^i = (\mathbf{H}\mathbf{x}^i - \mathbf{r})$ is the residue vector at the i -th iteration.

Figure 7 shows the evolution of the RMS error as a function of the iteration index, for four different μ values, when the occupancy level was kept fixed at 30%. When evaluating the dependency with respect to the parameter μ , the other parameter (λ) was set to zero. For these plots, the entire set (100.100 samples) was used to increase the statistics and no error bar is shown.

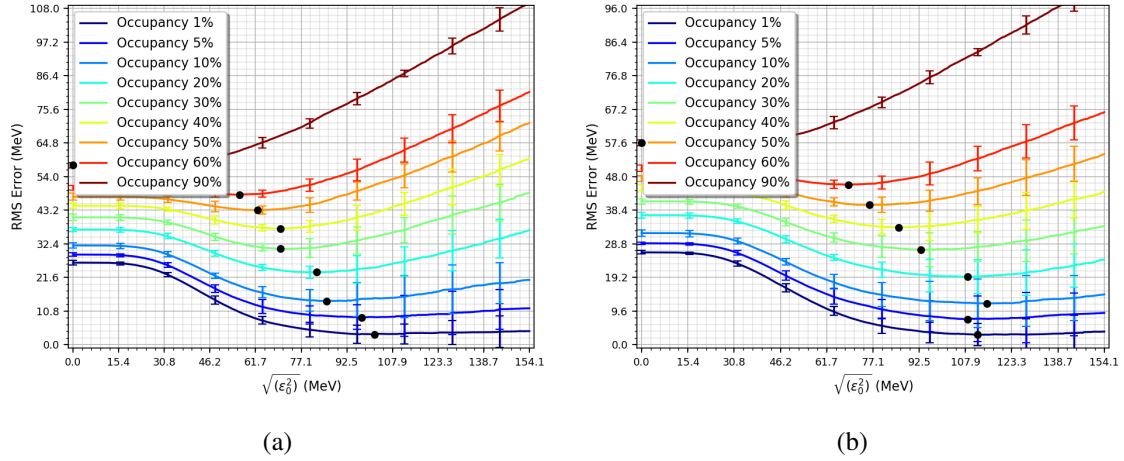


Figure 6: The RMS error as a function of the residue energy for both OMP (a) and LS-OMP (b) methods. The black dots point out the threshold values for which the minimum RMS errors were achieved.

The four evaluated values for μ were: the dynamic one (according to Equation 4.2) and three fixed values, in order to avoid the computation of Equation 4.2 in hardware. The three fixed values were chosen within the range of the values obtained through the dynamic approach, so that no multiplication circuitry would be necessary in a fixed-point numerical representation for any of these values in hardware (bit-shifting operation only) [57]. One may notice that $\mu = 0.5$ was too high and the algorithm turned out to be unstable. On the other extreme, for $\mu = 0.125$ the convergence was too slow. The best solution was found for $\mu = 0.25$, which produced an evaluation performance similar to the dynamical one (see Figure 7). Figure 8 summarises the SSF method performance as a function of the number of iterations for different occupancy levels, when $\mu = 0.25$ was kept fixed.

Concerning the tuning for the parameter λ , Figure 9 shows how the estimation performance behaved around the optimal value for several occupancy levels. It can be seen that the value of the parameter λ tended to zero while the pile-up level increased. Therefore, for sake of hardware simplicity, the parameter λ was set to zero, regardless the occupancy level.

The results in Figure 8 were obtained by initializing the vector \mathbf{x}^0 with the 48 central elements of the measured vector \mathbf{r} . This was shown to be faster than initializing \mathbf{x}^0 as a null vector. However, as it can be seen from this figure, more than 200 iterations were still necessary for algorithm convergence for most of the occupancy levels. Thus, in this work, the initialization of \mathbf{x} is proposed to follow Equation 3.12 and Figure 10 compares the evaluation of the estimation error as the number of iterations increases, with and without this pre-processing scheme, for a run with 30% of occupancy level. One can notice that the convergence proved to be faster when the proposed initialization was applied.

4.4 Estimation Performance

Once the parameters for the aforementioned methods were all set to their design tuned values, a performance comparison was carried out. Table 1 summarizes the final performance. In this table,

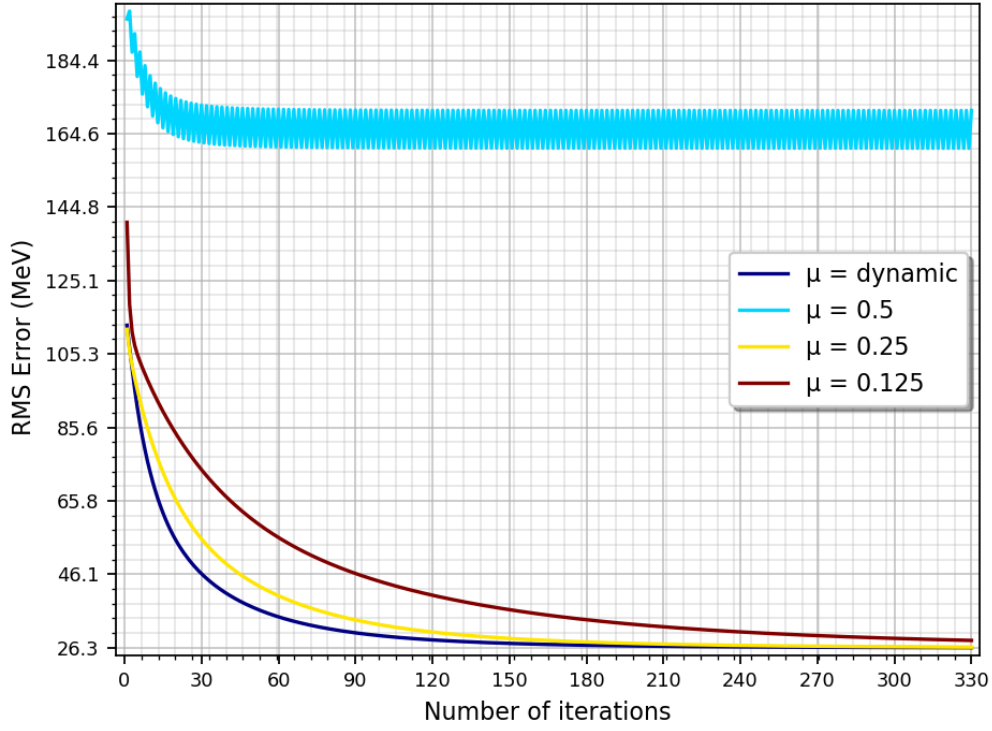


Figure 7: The RMS error as a function of the number of iterations. A run with 30% of occupancy level was employed.

LP (as described in [18]) corresponds to a direct implementation of the problem P_{1,ϵ_0} (Equation 3.9), and FIR corresponds to the method proposed in [23]. The last three columns refer to the methods proposed in this paper.

Table 1: Estimation performance in terms of the RMS error values (in MeV). Best performance for each occupancy level case is shown in boldface.

Occupancy level	LP	FIR Filter	OMP	LS-OMP	SSF*
1 %	4.44±1.07	15.22±2.33	3.27±0.75	2.86±0.49	3.72±0.33
5 %	10.13±0.67	18.48±0.91	8.77±0.56	7.29±0.35	9.21±0.62
10 %	14.9±0.93	22.3±0.74	13.95±0.9	11.8±0.91	13.28±0.84
20 %	22.12±0.83	29.76±0.68	23.27±0.64	19.36±0.79	20.51±0.92
30 %	28.47±0.9	35.33±0.69	30.79±1.03	27.12±0.73	26.26±0.82
40 %	34.32±0.92	40.27±0.65	37.26±0.86	33.45±0.93	31.67±0.9
50 %	39.03±0.91	44.12±0.7	43.25±1.09	39.91±0.83	36.57±0.68
60 %	45.6±0.97	47.72±0.8	48.17±0.77	45.67±0.97	41.01±0.98
90 %	59.21±0.87	54.15±0.76	57.68±0.88	57.68±0.88	52.63±0.65

*SSF parameters set as $\mu = 0.25$ and $\lambda = 0$

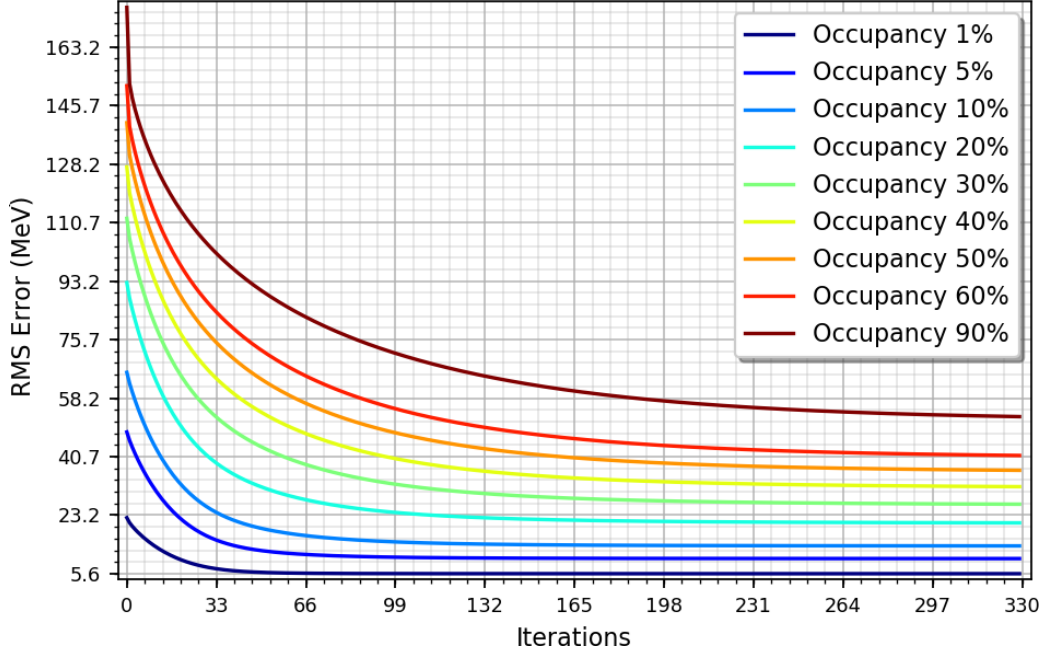


Figure 8: The RMS error as a function of the number of SSF iterations for several occupancy levels and $\mu = 0.25$.

For lower occupancy levels, the target sequence ($x[n]$) presented high sparsity and the SR methods outperformed the FIR filter considerably. As the occupancy level was increased, the sparsity assumption gradually lost its strength and the FIR filter performance got closer to the one from SR for occupancy values above 30%. Among the MP methods, LS-OMP was slightly better. The MP methods were less efficient with respect to SSF for higher occupancy levels. The first step of the MP algorithms, the vector support determination, presented lower efficiency when the sparsity of the target sequence was not so high. Concerning the offline method used for comparison (LP), the achieved results were similar to the ones from LS-OMP.

4.5 Detection Efficiency

In this section, performance evaluation in terms of detection efficiency is outlined. The analysis was performed through the Receiver Operating Characteristic (ROC) curve [58], which shows how the Probability of Detection (PD) for a given signal varies when a detection threshold is applied in the energy estimation value and the corresponding impact in the False Alarm (FA) probability. Here, PD comprised the percentage of BCs with hits that were correctly detected (estimated energy above the threshold) and FA was the percentage of BCs with no hits that have been wrongly selected. Figure 11 presents the ROC curves for two different occupancy levels (1% and 30%). The two tested MP methods (OMP and LS-OMP) presented similar results. Thus, only LS-OMP is shown in this analysis. For 1% of occupancy, both FIR filter and SSF methods presented similar detection efficiency. As the occupancy was increased, as 30%, for example, the advantage of the SR methods, when compared to the FIR filter, became more evident. The SSF method remained as one with the highest detection efficiency, regardless the occupancy level (1% or 30%).

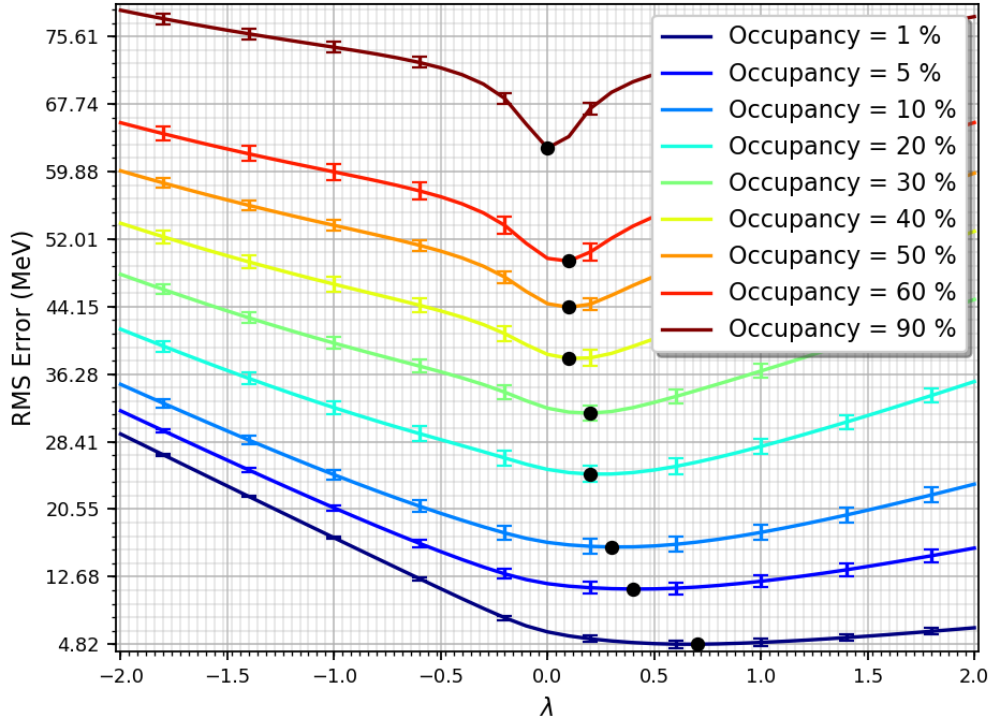


Figure 9: The RMS error as a function of the SSF parameter λ for several occupancy levels and $\mu = 0.25$. A total of 330 iterations were applied in order to guarantee full convergence of the algorithm. The black dots refer to the optimal values.

4.6 Analysis Summary

From the above analysis, one can conclude that, for lower occupancy conditions, if only the detection efficiency is taken into account (triggering purpose only), the FIR filter structure is a competitive choice, as it can be seen from the ROC curves. On the other hand, if the estimation accuracy is also an important issue, MP methods may be employed. For high pile-up levels, the SSF method may be chosen when both estimation accuracy and detection efficiency are of main concern. Besides, even for lower occupancy values the SSF method has shown to be competitive with respect to performance.

The SSF method has also lower computational cost, when compared to the MP algorithms. Therefore, the next section proposes an online implementation of the SSF method in FPGA technology and does a comparison with the FIR filter implementation in terms of technology resource requirements.

5 Hardware Implementation

Aiming at optimizing the hardware resource utilization, the argument in Equation 3.11 is rewritten according to:

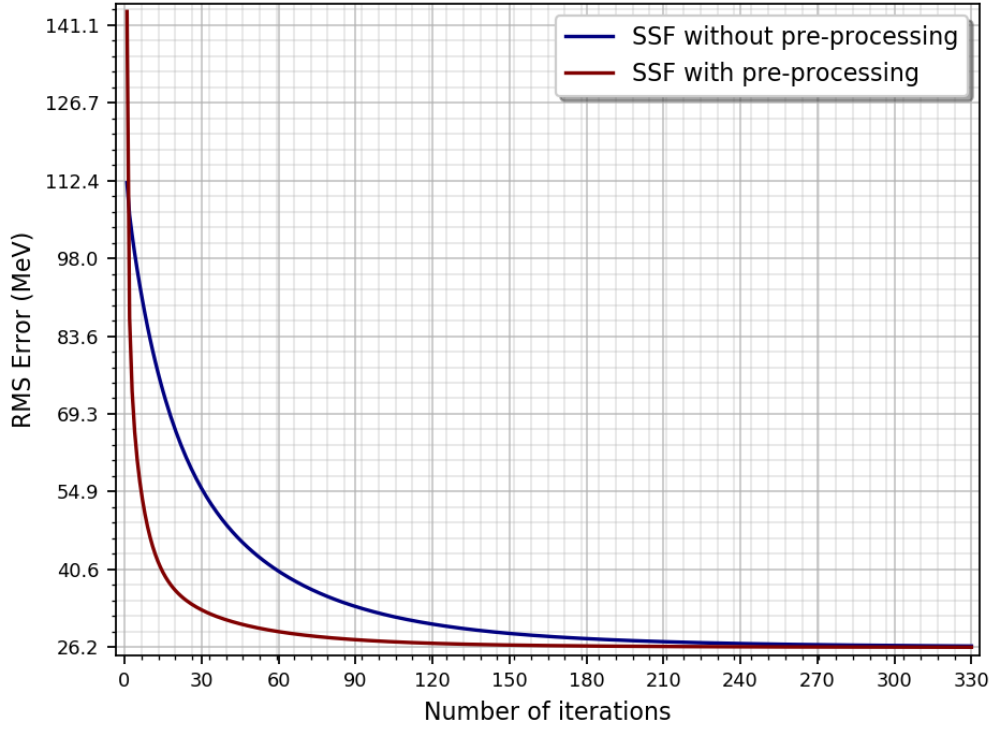


Figure 10: The RMS error as a function of the number of SSF iterations with and without the pre-processing step for \mathbf{x}^0 determination. A run with 30% of occupancy level was employed.

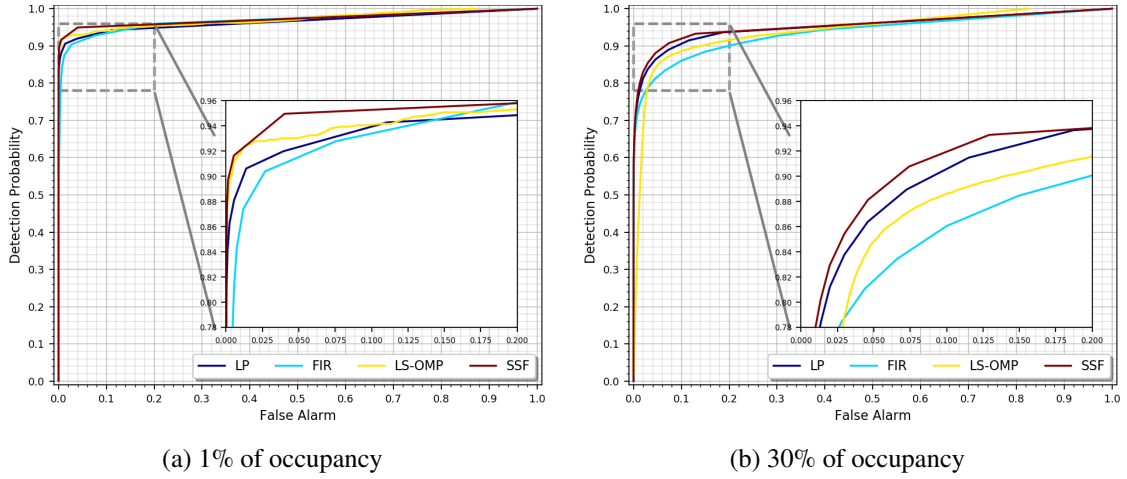


Figure 11: The ROC curves for low (a) and high (b) occupancy values.

$$\mathbf{x}^i + \mu(\mathbf{H}^T \mathbf{r} - \mathbf{H}^T \mathbf{H} \mathbf{x}^i) \quad (5.1)$$

where $\mathbf{H}^T \mathbf{H}$ is a constant Toeplitz matrix [59], which is computed offline. Concerning logic circuitry allocation, the Toeplitz matrix presents a certain symmetry that allows to reduce the cost through parallel implementation. In the text and in the figures that follow, this matrix is identified as \mathbf{Y} for

sake of simplicity. For the same reason, the vector $\mathbf{H}^T \mathbf{r}$ is also previously computed in hardware, just before the first iteration, and it will be indicated as a constant vector \mathbf{f} .

Other important simplification concerns the non-linearity imposed by the shrinkage function (Figure 3). For $\lambda = 0$, this function is implemented by a simple logic comparison: if the value is lower than zero, the component of the vector \mathbf{x} is replaced by zero before the next iteration.

Figure 12 shows the block diagram for SSF algorithm implementation. The blocks in gray color execute matrix computations altogether, in parallel (distributed combinational circuitry) and in fixed-point arithmetic [60]. In this figure, it is possible to identify a system with three pipeline stages [61], split into input and output register banks, where:

1. The first pipeline stage comprises the SIPO (Serial-Input Parallel-Output) circuitry, the block which computes the $\mathbf{f} = \mathbf{H}^T \mathbf{r}$ operation and the pre-processing for \mathbf{x}^0 computation. The SIPO assembles a window of 54 samples (the vector \mathbf{r}) buffering the most recent consecutive $r[n]$ samples. When the SIPO internal registers are fully occupied, both vectors \mathbf{f} and \mathbf{x}^0 are computed. In the next clock rising edge, the 48 resulting components, for both vectors, are stored in input register banks. This process is repeated to each window (54 clock cycles) uninterruptedly.
2. The second pipeline stage comprises the blocks between the input and the output register banks. The ones in gray color are responsible to execute one SSF iteration. This stage has a feedback path, synchronous to the data clock (40 MHz), in order to compute several iterations before the next window is delivered by the first pipeline stage. The resulting reconstructed vector (\mathbf{x}^i) is updated in the output register bank to each clock.
3. The third and last stage is executed by the PISO (Parallel-Input Serial-Output) block. This circuitry serialises the reconstructed vector present in the output register bank, delivering the free-running $\hat{x}[n - \Delta]$ information, synchronous with the ADC clock (40 MHz). In this way, the windowed processing of the proposed system becomes transparent.

5.1 System Evaluation

As described before, the system operates in a three stage pipeline architecture. Thus, three consecutive windows are evaluated simultaneously, one at each stage. The first stage buffers the most recent window and sends the data, in parallel, to the next stage.

The SSF iterations are implemented by the second pipeline stage. In the first clock, the multiplexer is switched to the input register. In this way, the initial value of the algorithm is \mathbf{x}^0 , as expected. This signal propagates through the blocks that compute one SSF iteration. For the consecutive 53 clock cycles, the multiplexer points to the output register, which updates the reconstructed vector, in a feedback data-flow, at each clock cycle. In this stage, if only one SSF iteration block is implemented, it is possible to compute 54 iterations before the first stage sends a new fresh window. Therefore, a cascade of z blocks allows the execution of $54 \times z$ iterations.

Last stage simply serializes the most recent reconstructed window delivered by the second stage. As a consequence of this proposed architecture, the response delay Δ is fixed in 2 times the window size ($2 \times 54 = 108$), regardless the number of iterations (which is a multiple of 54).

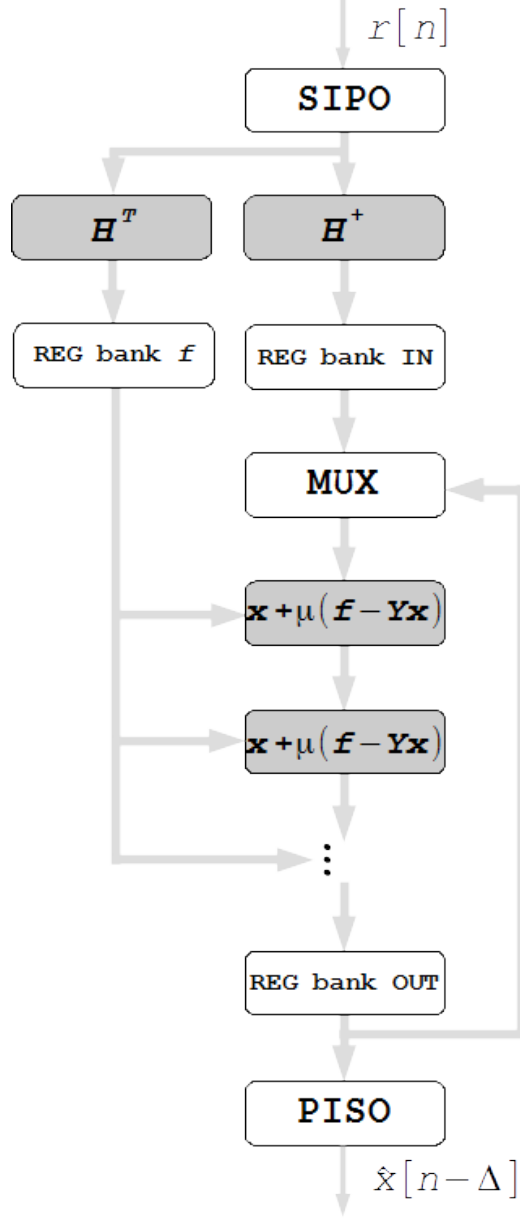


Figure 12: The block diagram of the proposed circuitry. It operates synchronously with the $r[n]$ input signal.

5.2 FPGA Implementation

The proposed circuitry was implemented in FPGA. The Software Vivado [62] was used in the design, and Verilog [63] as Hardware Description Language (HDL) [64]. For performance tests, the chip XCZU7EV-FFVC1156-2-E from the Zynq UltraScale+ family [65] was chosen, since its evaluation is free and can be crosschecked without costs. For representation, 17 bits (7 bits for range and 10 bits for precision) were selected for fixed-point arithmetic, for all the parts of the circuitry. This configuration was chosen empirically after exhaustive simulation with several different numerical representations. Table 2 summarizes the implementation performance. As for comparison, the

results for a FIR filter structure are also outlined. In this table, it is shown performance results for up to three cascaded iteration blocks. For more than this, the operation frequency is below 40 MHz. Among the SSF implementations, the one with only one iteration block together with the pre-processing circuit is an attractive solution in terms of cost-benefit.

Table 2: Implementation resources in terms of different hardware elements and frequency operation.

Metrics	FIR	SSF 1 Block		SSF 2 Blocks		SSF 3 Blocks	
		Pp	nPp	Pp	nPp	Pp	nPp
LUT**	1,447	31,378	33,132	59,927	63,966	87,160	94,870
FF**	731	2,097	2,625	2,098	2,625	2,097	2,625
DSP**	125	435	308	503	376	571	444
Freq (MHz)	56.76	71.20	79.17	50.34	57.39	41.47	42.22
RMS (MeV)	40	31	43	29	32	28	29

Pp = with pre-processing nPp = without pre-processing

***Number of: LUT = Look-up-tables, FF = Flip-Flops, DSP = Digital Signal Processor*

6 Conclusion

This paper presented an iterative method for a matrix based deconvolution process, which can be implemented for online operation. The proposed method is based on established sparse theory, overperforming the previously proposed FIR filter based deconvolution method. The method based on Iterative Shrinkage has shown to be a good choice for implementation and a FPGA circuitry was proposed. Comparing with FIR filter design, although the cost implementation increases, it looks feasible when modern FPGA technology is considered. The gain in performance is expressive, and it can justify its usage in experiments with intense pile-up levels.

Acknowledgment

The authors would like to thank CNPq, CAPES, RENAFAE-MCTI, FAPERJ, FAPEMIG (Brazil) and CERN (Switzerland) for their support to this work.

References

- [1] W. Barletta, M. Battaglia, M. Klute, M. Mangano, S. Prestemon, L. Rossi et al., *Future Hadron Colliders: from physics perspectives to technology R&D*, *Nucl. Instrum. Methods Phys. Res., A* **764** (Jan, 2014) 352–368. 17 p.
- [2] O. Brüning and L. Rossi, *The High Luminosity Large Hadron Collider*. WORLD SCIENTIFIC, Geneve, 2015, [10.1142/9581](#).
- [3] L. Evans and P. Bryant, *Lhc machine*, *Journal of Instrumentation* **3** (2008) S08001.
- [4] K. Anthony, *Celebrating the first of a kind*, *CERN Document Server* (sep, 2014) .
- [5] C. Pralavorio, *The new annual report is available*, *CERN Document Server* (jun, 2017) .

- [6] M. Cepeda, S. Gori, P. Ilten and Collaboration, *Report from Working Group 2: Higgs Physics at the HL-LHC and HE-LHC*, [*CERN Yellow Rep. Monogr.* **7** \(Dec, 2018\) 221–584. 364 p.](#)
- [7] ATLAS COLLABORATION collaboration, W. Walkowiak, *ATLAS Plans for the High-Luminosity LHC*, Tech. Rep. ATL-PHYS-PROC-2018-048, CERN, Geneva, Jun, 2018. 10.22323/1.326.0055.
- [8] R. Wigmans, *Calorimetry*. Oxford University Press, 2nd edition ed., Jan, 2018, [10.1093/oso/9780198786351.001.0001](#).
- [9] M. Jeitler, *Trigger systems of LHC experiments*, [*Journal of Instrumentation* **12** \(may, 2017\) C05012–C05012.](#)
- [10] ATLAS collaboration, G. Aad et al., *The atlas experiment at the cern large hadron collider*, [*Journal of Instrumentation* **3** \(2008\) S08003.](#)
- [11] CMS collaboration, S. Chatrchyan et al., *The cms experiment at the cern lhc*, [*Journal of Instrumentation* **3** \(2008\) S08004.](#)
- [12] E. Fullana, J. Castelo, V. Castillo, C. Cuenca, A. Ferrer, E. Higon-Rodriguez et al., *Digital signal reconstruction in the atlas hadronic tile calorimeter*, [*Nuclear Science, IEEE Transactions on* **53** \(09, 2006\) 2139 – 2143.](#)
- [13] V. Radeka and S. Rescia, *Speed and noise limits in ionization chamber calorimeters*, [*Nuclear Instruments and Methods in Physics Research Section A: Accelerators, Spectrometers, Detectors and Associated Equipment* **265** \(Mar, 1988\) 228–242.](#)
- [14] G. Bertuccio, E. Gatti, M. Sampietro, P. Rehak and S. Rescia, *Sampling and optimum data processing of detector signals*, [*Nuclear Instruments and Methods in Physics Research Section A: Accelerators, Spectrometers, Detectors and Associated Equipment* **322** \(Nov, 1992\) 271–279.](#)
- [15] W. Cleland and E. Stern, *Signal processing considerations for liquid ionization calorimeters in a high rate environment*, [*Nuclear Instruments and Methods in Physics Research Section A: Accelerators, Spectrometers, Detectors and Associated Equipment* **338** \(Jan, 1994\) 467–497.](#)
- [16] L. M. de Andrade Filho, B. S. Peralva, J. M. de Seixas and A. S. Cerqueira, *Calorimeter response deconvolution for energy estimation in high-luminosity conditions*, [*IEEE Transactions on Nuclear Science* **62** \(Dec, 2015\) 3265–3273.](#)
- [17] S. Haykin, *Adaptive Filter Theory*. Prentice Hall, NJ, USA, 5th edition ed., 2013.
- [18] D. P. Barbosa, L. M. d. A. Filho, B. S. Peralva, A. S. Cerqueira and J. de Seixas, *Sparse representation for signal reconstruction in calorimeters operating in high luminosity*, [*IEEE Transactions on Nuclear Science* **64** \(Jul, 2017\) 1942–1949.](#)
- [19] M. Elad, *Sparse and Redundant Representations*. Springer New York, New York, 2010, [10.1007/978-1-4419-7011-4](#).
- [20] L. R. M. Silva, L. M. de Andrade Filho and C. A. Duque, *Sparse representation algorithm applied to power systems signal compression*, [*International Transactions on Electrical Energy Systems* **29** \(Aug, 2018\) e2693.](#)
- [21] J.-L. Starck, F. Murtagh and J. M. Fadili, *Sparse Image and Signal Processing: Wavelets, Curvelets, Morphological Diversity*. Cambridge University Press, New York, 2010.
- [22] S. K. Mitra, *Digital Signal Processing : A Computer-Based Approach*. McGraw-Hill Higher Education, New York, 4th edition ed., 2010.
- [23] J. Duarte, L. de Andrade Filho, E. de Simas Filho, P. Farias and J. de Seixas, *Online energy*

reconstruction for calorimeters under high pile-up conditions using deconvolutional techniques, *Journal of Instrumentation* **14** (dec, 2019) P12017–P12017.

- [24] S. H. Lim, J. Won Choi and B. Shim, *Greedy sparse channel estimation for millimeter wave communications*, in *TENCON 2018 - 2018 IEEE Region 10 Conference*, pp. 1628–1632, Oct, 2018. DOI.
- [25] A. Zaki, A. Venkitaraman, S. Chatterjee and L. K. Rasmussen, *Greedy sparse learning over network*, *IEEE Transactions on Signal and Information Processing over Networks* **4** (Sep, 2018) 424–435.
- [26] M. Niu, W. Li, Z. Liu, Y. Zhang and J. Yang, *An accelerated iterative shrinkage-thresholding algorithm for real-beam scanning radar super-resolution*, in *2019 IEEE Radar Conference (RadarConf)*, pp. 1–4, Apr, 2019. DOI.
- [27] Y. Ma and T. Zheng, *Stabilized sparse online learning for sparse data*, 2017.
- [28] P. Zhao, D. Wang, P. Wu and S. C. H. Hoi, *A unified framework for sparse online learning*, *ACM Trans. Knowl. Discov. Data* **14** (Aug., 2020) .
- [29] TEVATRON BEAM-BEAM TEAM collaboration, V. Shiltsev, *Overview of beam-beam effects in the Tevatron*, in *Proceedings, ICFA Mini-Workshop on Beam-Beam Effects in Hadron Colliders (BB2013): CERN, Geneva, Switzerland, March 18-22 2013*, pp. 11–18, 2014. 1410.3326. DOI.
- [30] W. Herr, *Dynamic behaviour of nominal and pacman bunches for different lhc crossing schemes*, Tech. Rep. LHC-Project-Report-856. CERN-LHC-Project-Report-856, CERN, 01, 2005.
- [31] J. Fox, H. Bartosik, E. Bjørsvik, S. De Santis, J. Dusatko, W. Höfle et al., *Control of Intra-Bunch Vertical Motion in the SPS with GHz Bandwidth Feedback*, *J. Phys. : Conf. Ser.* **1067** (2018) WEPAL079. 6 p.
- [32] M. Hostettler, K. Fuchsberger, G. Papotti, Y. Papaphilippou and T. Pieloni, *Luminosity Scans for Beam Diagnostics*, *Phys. Rev. Accel. Beams* **21** (Apr, 2018) 102801. 10 p.
- [33] E. Candes and T. Tao, *The dantzig selector: Statistical estimation when p is much larger than n* , *Ann. Statist.* **35** (12, 2007) 2313–2351.
- [34] D. G. Luenberger and Y. Ye, *Linear and Nonlinear Programming*. Springer US, New York, 2008.
- [35] S. G. Mallat and Zhifeng Zhang, *Matching pursuits with time-frequency dictionaries*, *IEEE Transactions on Signal Processing* **41** (Dec, 1993) 3397–3415.
- [36] D. R. Hadley, *Digital filtering performance in the ATLAS level-1 calorimeter trigger*, in *Real Time Conference (RT), 2010 17th IEEE-NPSS*, pp. 1–6, IEEE, 2010.
- [37] S. M. Kay, *Fundamentals of Statistical Signal Processing, Volume I*. Prentice Hall, NJ, USA, 1993.
- [38] S. Chen and M. Yang, *An adaptive fast iterative shrinkage threshold algorithm*, in *2017 29th Chinese Control And Decision Conference (CCDC)*, pp. 2190–2194, May, 2017. DOI.
- [39] M. Takac, *Randomized Coordinate Descent Methods for Big Data Optimization*. University of Edinburgh, Edinburgh, 2014.
- [40] U. Meyer-Baese, *Digital Signal Processing with Field Programmable Gate Arrays*. Springer Berlin Heidelberg, New York, 3 ed., 2007, 10.1007/978-3-540-72613-5.
- [41] G. Arce, *Nonlinear signal processing : a statistical approach*. Wiley-Interscience, Hoboken, N.J, 2005.
- [42] H. Wu and S. Wang, *Adaptive sparsity matching pursuit algorithm for sparse reconstruction*, *IEEE Signal Processing Letters* **19** (2012) 471–474.

- [43] T. T. Cai and L. Wang, *Orthogonal matching pursuit for sparse signal recovery with noise*, *IEEE Transactions on Information Theory* **57** (2011) 4680–4688.
- [44] B. Dumitrescu, *Sparse total least squares: Analysis and greedy algorithms*, *Linear Algebra and its Applications* **438** (Mar, 2013) 2661–2674.
- [45] C. T. Kelley, *Solving Nonlinear Equations with Newton's Method*. Society for Industrial and Applied Mathematics, Jan, 2003, [10.1137/1.9780898718898](https://doi.org/10.1137/1.9780898718898).
- [46] I. Daubechies, M. Defrise and C. De Mol, *An iterative thresholding algorithm for linear inverse problems with a sparsity constraint*, *Communications on Pure and Applied Mathematics: A Journal Issued by the Courant Institute of Mathematical Sciences* **57** (2004) 1413–1457.
- [47] S. Yun, *A Coordinate Gradient Descent Method for Structured Nonsmooth Optimization: Theory and Applications*. VDM Verlag Dr. Müller, Dec, 2010.
- [48] S. Roman, *Advanced linear algebra*. Springer, New York, 2008.
- [49] I. Hrivnacova, D. Adamova, V. Berejnoi, R. Brun, F. Carminati, A. Fasso et al., *The Virtual Monte Carlo*, *CERN Document Server* (May, 2003) 8 p.
- [50] J. Chapman, *ATLAS simulation computing performance and pile-up simulation in ATLAS*, *LPCC* (2011) .
- [51] CMS COLLABORATION collaboration, S. Banerjee, *CMS Simulation Software*, Tech. Rep. CMS-CR-2012-146, CERN, Geneva, Jun, 2012. [10.1088/1742-6596/396/2/022003](https://doi.org/10.1088/1742-6596/396/2/022003).
- [52] B. S. M. Peralva, L. M. A. Filho, A. S. Cerqueira and J. M. Seixas, *The TileCal Energy Reconstruction for Collision Data Using the Matched Filter*, in *2013 IEEE Nuclear Science Symposium and Medical Imaging Conference (2013 NSS/MIC)*, pp. 1–6, 2013. [DOI](https://doi.org/10.1109/NSSMIC.2013.6746111).
- [53] Y. Sugiyama, J. Xu, M. Tecchio, N. Whallon, D. McFarland, J. Ma et al., *The data acquisition system for the koto experiment*, *IEEE Transactions on Nuclear Science* **62** (Jun, 2015) 1115–1121.
- [54] J. Keil, *Operational experience with hera*, in *2007 IEEE Particle Accelerator Conference (PAC)*, pp. 1932–1934, Jun, 2007. [DOI](https://doi.org/10.1109/PAC.2007.4317111).
- [55] R. Duda, P. Hart and D. G. Stork, *Pattern Classification*, vol. xx, p. 654. John Wiley and Sons, inc, 01, 2001.
- [56] D. P. Bertsekas, *Nonlinear Programming*. Athena Scientific, Sep, 1999.
- [57] W. E. Milne, *Numerical Calculus (Princeton Legacy Library)*. Princeton University Press, Apr, 2016.
- [58] T. Fawcett, *An introduction to ROC analysis*, *Pattern Recognition Letters* **27** (Jun, 2006) 861–874.
- [59] A. Böttcher and S. M. Grudsky, *Toeplitz Matrices, Asymptotic Linear Algebra and Functional Analysis*. Hindustan Book Agency, 2000, [10.1007/978-93-86279-04-0](https://doi.org/10.1007/978-93-86279-04-0).
- [60] W. T. Padgett and D. V. Anderson, *Fixed-point signal processing*, *Synthesis Lectures on Signal Processing* **4** (Jan, 2009) 1–133.
- [61] Y. Oda and T. Oyama, *Fast calculation using parallel processing and pipeline processing in power system analysis*, *Electrical Engineering in Japan - ELEC ENG JPN* **116** (Jan, 1996) 85–96.
- [62] S. Churiwala, *Designing with Xilinx FPGAs: Using Vivado*. Springer Publishing Company, Incorporated, 1st ed., 2016.
- [63] S. Monk, *Programming FPGAs : getting started with Verilog*. McGraw Hill Education, New York, NY, 2017.

- [64] N. Botros, *Hdl with Digital Design*. Mercury Learning & Information, 2015.
- [65] Xilinx, *Zynq ultrascale+ device packaging and pinouts*, 2020.